Mem. S.A.It. Vol. 81, 974

Memorie della

The upper mass limit for the formation of TP–SAGB stars and the dredge–out phenomenon

P. Gil–Pons[1,2] and C. L. Doherty[1]

[1] Universitat Politecnica de Catalunya – Department of Applied Physics, Campus Baix Llobregat, Building C3, 08860 Castellefels, Spain, e-mail: pilar@fa.upc.edu

[2] Centre for Stellar and Planetary Astrophysics, School of Mathematical Sciences, Monash University, Victoria 3800, Australia

Abstract. We have computed the evolution of Super-AGB stars from the main sequence and up to a few hundred thermal pulses, with special attention to the low metallicity cases ($Z = 10^{-10}, 10^{-5}, 10^{-4}$ and 10^{-3}). Our computations have been performed using time–dependent mixing and new opacity tables that admit variations in the abundances of carbon and oxygen. By following the evolution along the main central burning stages and the early TP-SAGB, we resolve the upper mass limits for the formation of TP-SAGB stars and determine the mass range at which the dredge-out phenomenon occurs. This phenomenon involves the merger of a convective shell sustained by helium burning at the top of the degenerate core with the hydrogen–rich convective envelope and the occurrence of a hydrogen flash. The dredge–out allows elements synthesised through helium burning to be transported to the stellar surfaces and therefore it can affect the initial composition of the TP-SAGB stars.

Key words. Stars: abundances – Stars: Population II – Stars: Population III

1. Introduction

Super-AGB stars develop central hydrogen and helium burning and finally carbon burning in a degenerate core. They are the most massive stars that evolve along the thermally pulsing phase. As it has been shown by former works, Doherty et al. (2010), Siess (2007, 2009), Gil–Pons et al. (2007), the mass range for the formation of Super-AGB stars depends on the initial metallicity and on the physics and numerical details of the evolutionary codes, but it ranges approximately between 7 and 11 $M_{\odot}$.

Computing the evolution of Super-AGB stars involves a considerable computational effort, not only because carbon–burning in a series of flashes must be followed, but also because of the large number of thermal pulses that these stars go through –from hundreds or even thousands. They also pose an additional challenge, as it is not clear that they always end their lives as oxygen–neon white dwarfs. Instead, the most massive of these objects might end their lives as supernovae, and the minimum initial mass value for Super–AGB stars to become supernovae is expected to depend on their initial metallicity. To sum-

Send offprint requests to: P. Gil-Pons marise, in spite of the effort that has already been made for their understanding, the contribution of Super–AGB stars to the chemical evolution of the universe is still unknown.

The present work considers the determination of the upper mass limit for the formation of TP-SAGB stars as a function of the initial metallicity. This involves the computation of the so–called dredge–out episode, in which regions processed by helium–burning are mixed with the convective envelope of the stars at time scales much shorter than the turnover timescale of the convective envelope.

As we describe in the second section of this paper our computations have been carried out using the MONSTAR evolutionary code. In the third section we describe the dredge-out phenomenon, determine its dependance on the initial metallicity of the stars, and establish a relation between the initial mass of the stars and the size of the degenerate cores they develop after carbon–burning. In the fourth section we determine the lower mass limit for the formation of degenerate cores below M_{Ch} at the end of the carbon burning phase. In the fifth section we compare the evolution of the surface metallicities of $Z = 10^{-5}$ stars of different masses, to see the differences between a star that has undergone the dredge–out phenomenon and stars that have undergone a standard second dredge–up. Finally in the last section we derive the main conclusions of our work.

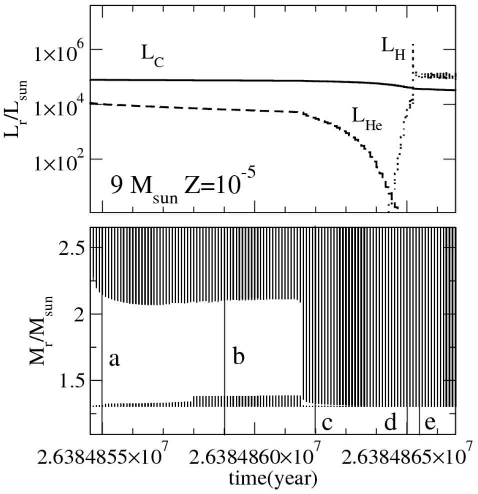

Fig. 1. Upper panel: Evolution of the luminosities associated to hydrogen (L_H), helium, (L_{He}) and carbon burning (L_C). Lower panel: evolution of the convective shell and the convective envelope. Both panels correspond to the last stages of the carbon burning phase and the dredge-out process.

2. Brief description of the code

The calculations presented in this work have been made using the MONSTAR code, that is the Monash version of EVOLN -the Mount Stromlo Stellar Structure code. MONSTAR includes only the isotopes that are relevant for the structural evolution of stars, but its output can be used to obtain the evolution of detailed nucleosynthesis -up to 116 isotopes from hydrogen to iron, through the DPPNS45 code, also developed at Monash University. MONSTAR has been updated to include the new opacity tables (Rogers & Iglesias 1996) with variable carbon and oxygen abundances, as well as the molecular opacities for the low temperature cases (Ferguson et al. 2005). At higher densities and temperatures, the conductive opacities used are from Potekhin (1999). Neutrino losses are computed according to Itoh et al. (1996).

Time–dependent mixing has been implemented in MONSTAR by Campbell (2007). The diffusion equation is solved using implicit finite differences, as explained in Meynet et al. (2004). This treatment of mixing allows us to compute the dredge-out because, as we will explain later, this process involves evolutionary time scales comparable to the time of the convective turnover for the convective envelope.

3. The dredge-out as a function of the initial metallicity

The dredge-out process was first described in the literature by Ritossa et al. (1999). It occurs at the end of the carbon–burning phase of Super–AGB stars, and involves the advance inwards of the hydrogen–rich convective envelope and the advance outwards of the convec-

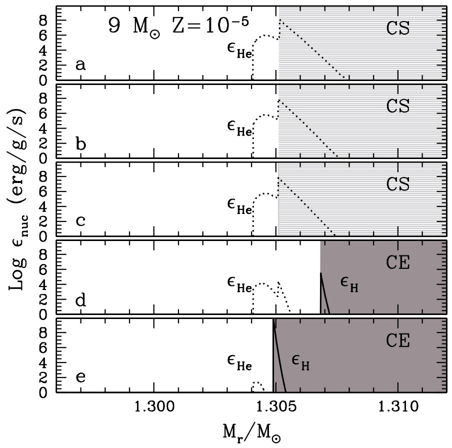

Fig. 2. Energy generation rates due to hydrogen burning (ϵ_H, in solid lines) and helium burning (ϵ_{He}, in dotted lines) at the times specified in Fig. 1. The shaded areas represent convection in a shell (CS) and in the hydrogen–rich envelope (CE).

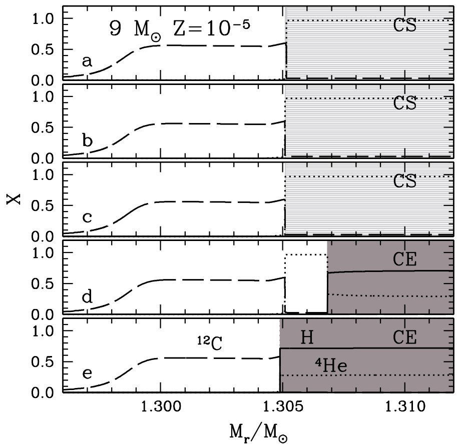

Fig. 3. Hydrogen (solid), helium (dotted) and carbon abundances (dashed) at the different times specified in Fig. 1. The shaded areas represent convection in a shell (CS) and in the hydrogen–rich envelope (CE).

tive shell associated to helium burning. When these zones merge, protons are ingested in regions of high density and temperature and, then, a hydrogen flash occurs. The ingestion of protons and the occurrence of the hydrogen flash take place in time scales that are of the order of, or shorter than, the convective turnover timescale. Therefore, a time dependant mixing formalism is required in order to compute this process.

The characteristic time scales are an important difference between the dredge–out (DO) and a standard second dredge–up process (2DU), in which evolution takes place at characteristic timescales much longer than those of convective mixing and, therefore, the instant mixing approximation holds.

The second important difference between the 2DU and the DO is the composition of the regions that they affect. The 2DU mixes the convective envelope with matter processed by hydrogen burning, whereas the DO is also able to mix matter processed by helium burning.

The third important difference is that, as a consequence of this mixing of protons into very hot regions of the star, during the DO episodes a hydrogen flash occurs, unlike the cases in which only standard 2DU processes happen.

Fig. 1 represents the evolution of luminosity and convection during the dredge-out phase for our 9 $M_\odot$ $Z = 10^{-5}$ model star. The lower panel shows how the position of the base of the convective envelope (BCE) and of the inner convective shell sustained by helium–burning in a shell (shaded regions) advance. We can see at times *a* and *b* the coexistence of both convective zones. At time *c* the BCE advances inwards and reaches the convective shells, enriched in isotopes procesed by helium burning. This part of the evolution occurs in very short time scales –less than 1 year, and mixes protons into interior regions that are at high density and temperature. This causes the fast onset of a flash in the hydrogen–burning shell –see times *c* and *d*.

This burning shell reaches a peak luminosity above $10^6 L_\odot$ and allows the expansion and cooling of the surrounding regions and, in particular, of the helium–burning shell. Therefore helium burning switches off, and hydrogen and

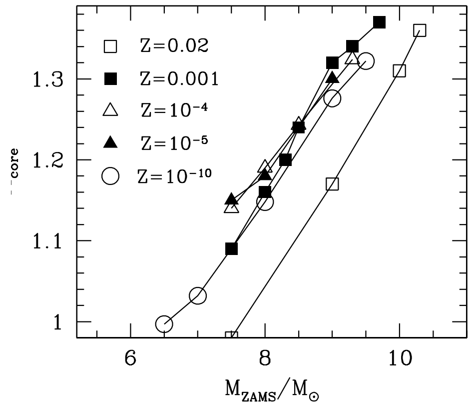

Fig. 4. Remnant core mass versus ZAMS mass relation for some of the computed models for the solar metallicity cases (represented with open squares), for the $Z = 10^{-3}$ cases (solid squares), for the $Z = 10^{-4}$ cases (open triangles), for the $Z = 10^{-5}$ cases (solid triangles) and for the $Z = 10^{-10}$ cases (open circles).

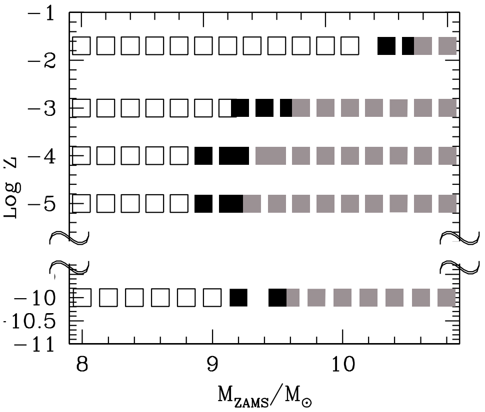

Fig. 5. Initial mass and metallicity for stars that develop degenerate cores less massive than M_{Ch} and undergo a standard second dredge–up episode (open squares); for stars that also develop degenerate cores less massive than M_{Ch}, but undergo a dredge–out process (black squares); and for stars that develop degenerate cores more massive than M_{Ch} (grey squares).

carbon burning remain the nuclear energy suppliers for the star during this phase of the evolution. Once the hydrogen flash is finished, hydrogen burning still remains active and burns *in situ* until the TP-SAGB phase starts.

Figs. 2 and 3 represent partial mass profiles of the 9 $M_{\odot}$ $Z = 10^{-5}$ model star at the times labelled in Fig. 1. Fig. 2 shows the logarithm of the energy generation rates due to hydrogen and helium burning. From panel *a* to panel *c* we can see that helium burning sustains the convective shell –represented by the shaded region above the mass point $M_r = 1.30505 M_{\odot}$. At paneld *d* of Figs. 2 and 3 we can see that the BCE has advanced inwards to the helium–rich regions.

The ingestion of protons into high temperature and high density regions allows the onset of hydrogen burning at the BCE, and the associated expansion and cooling of the helium–burning shell causes a decrease in the helium–burning rates. Finally, at panel *e* of Figs. 2 and 3 the BCE has reached the outermost parts of the carbon–oxygen shell that surrounds the oxygen–neon core.

4. The lower mass threshold for the formation of ONe cores below the Chandrasekhar mass

We have obtained the relation between the initial mass of stars at different metallicities and the masses of their remnant degenerate cores at the end of carbon burning (Fig. 4).

The solar metallicity models (open squares) yield the lowest core masses, followed by the zero metallicity ones (open circles). $Z = 10^{-3}$ models (solid squares) yield somewhat more massive cores and finally $Z = 10^{-4}$ (open triangles) and $Z = 10^{-5}$ models (close triangles) tend to yield the most massive remnant cores. Anyway one can see in the figure that, for initial masses above 8 $M_{\odot}$, the remnant core masses yield almost the same values, independently of their initial metallicity, except for the solar case.

Stars that experience the dredge–out process are the most massive intermediate–mass stars that can become oxygen–neon white dwarfs, independently of their initial metallicity ($M_{n-\epsilon}$). Therefore, by computing this process, we are able to determine which stars will avoid a supernova explosion, at least before entering the TP-SAGB phase.

As we can see in Fig. 5, solar metallicity stars can develop ONe cores below the Chandrasekhar mass, from initial masses up to 10.7 $M_{\odot}$. Fig. 5 also shows the behaviour of $M_{n-\epsilon}$ with metallicity. $M_{n-\epsilon}$ decreases from solar metallicities down to Z=10^{-4} – 10^{-5} values. This behaviour was also observed by Siess (2007). In our case $M_{n-\epsilon}$ decreases from $10.7 M_{\odot}$ for the solar metallicity down to $9.3 M_{\odot}$ for the $Z = 10^{-4}$ case.

5. Evolution of the surface composition for the $Z = 10^{-5}$ cases

Fig. 6 represents the time evolution of convection (left panels) and surface compositions of carbon, nitrogen and oxygen (right panels) along carbon burning and the first tens of thermal pulses of the TP-SAGB phase for the $Z = 10^{-5}$ 7.5, 8, 8.5 and 9 $M_{\odot}$ models. On the right panels the carbon, nitrogen and oxygen surface abundances are represented with solid, dotted and dashed lines respectively.

The 7.5, 8 and 8.5 $M_{\odot}$ models undergo a normal second dredge–up process and the 9 $M_{\odot}$ model, as we have seen in Section 3 of this work, undergoes a dredge–out episode. The 7.5 $M_{\odot}$ model experiences a relatively mild second dredge–up and, because of the low metallicity, no first dredge–up at all. Therefore the total surface metallicity remains low, of the order of $Z = 10^{-5}$, even along carbon burning and the TP-SAGB phase.

The other models we have computed show an important increase in the surface metal abundance (two orders of magnitude with respect to the initial values) due to the second dredge–up (or dredge–out) process. The most massive model, that is, the $9 M_{\odot}$ case, shows a lower increase in surface metallicity, as the dredge–out process, even though it reaches regions of the star closer to the core, lasts a much shorter time than a standard second dredge–up. The fact that metals in this case have to be diluted in a larger hydrogen–rich envelope also favours this result. We can also see, very clearly, a decrease in carbon and oxygen and an increase of nitrogen due to hot bottom burning along the TP–SAGB.

As a general trend, according to our computations, all the models up to M_{ZAMS} about 8.5 $M_{\odot}$ show a slow increase with mass of the surface abundances of C, N, O. Specially for the $Z = 10^{-4}$ cases, the carbon abundance shows an increase of about 4 orders of magnitude with respect to the initial value and the oxygen abundance decreases significantly for initial masses lower than about 7 $M_{\odot}$. We will the develop this result further in a forthcoming work (Gil–Pons & Doherty 2010, in prep.).

6. Conclusions

We have computed the evolution of the central burning stages and the first tens of thermal pulses of the TP-(S)AGB phase of intermediate–mass stars from $7 M_{\odot}$ to $11 M_{\odot}$, of metallicities ranging from primordial to solar values. We have performed our calculations including time–dependent mixing. In particular, we have followed the dredge–out process, that occurs for all metallicities, in the most massive cases that develop degenerate cores below the Chandrasekhar mass after carbon burning. The dredge–out process is able to mix material processed by helium–burning with the hydrogen–rich convective envelope.

We have obtained the upper initial mass limits for the formation of oxygen–neon cores below the Chandrasekhar mass, ($M_{n-\epsilon}$), and show its dependance on metallicity. Minimum values for $M_{n-\epsilon}$ are reached for metallicities about $Z = 10^{-5} – Z = 10^{-4}$.

As pointed out by Tout & Eldridge (2004), Poelarends et al. (2006), Gil–Pons et al. (2007), or Siess (2007), the determination of the fate of stars in the mass range we have considered is a complex problem and, even though a star can develop a degenerate core below the Chandrasekhar mass after carbon burning, depending on the core growth rates, the convection and mixing schemes and the importance of the role of stellar winds during the TP–ASAGB phase, such star might become a supernova.

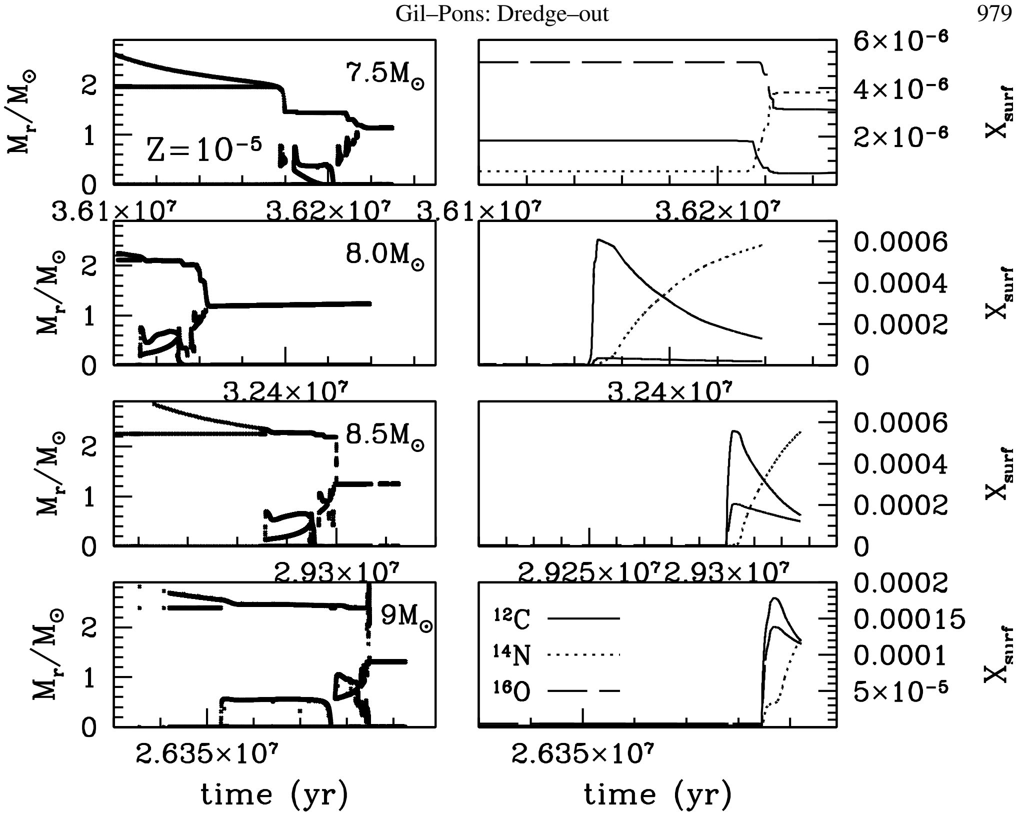

Fig. 6. Evolution of convection (left panels) and surface composition (right panels) from the second dredge–up for the 7.5, 8.0 and 8.5 $M_\odot$ models and including the dredge–out episode for the 9.0 $M_\odot$ model. On the right panels solid, dotted and discontinuous lines represent, respectively, the carbon, nitrogen and surface abundances. Carbon consistently appears to be the most abundant element for the 8, 8.5 and 9 $M_\odot$ models after the second dredge–up or dredge–out process.

References

Angulo, C., et al. 1999, Nucl. Phys. A, 656, 3

Campbell, S.W. 2007, PhD thesis, Monash University

Caughlan, G.R., & Fowler, W.A. 1988, At. Data Nucl. Data Tables, 40, 283

Doherty, C.L., Siess, L., Lattanzio, J.C., & Gil–Pons, P. 2010, MNRAS 401, 143

Ferguson, J.W., et al. 2005, ApJ 623, 585

Gil–Pons, P., Gutiérrez, J., Garcia-Berro, E. 2007, A & A 464, 767

Gil–Pons, P., Gutiérrez, J., Garcia-Berro, E. 2007, PoS, "Supernovae: lights in the darkness" 013

Gil–Pons, P., Doherty, C. L. 2010, in prep.

Itoh, N., Hayashi, H., Nishikawa, A., Kohyama, Y., 1996, ApJ 464, 943

Meynet, G., Maeder, A., Mowlavi, N., 2004, A&A 416, 1023

Poelarends, A. J. T., Izzard, R. G., Herwig, F., Langer, N., Heger, A., 2006, MmSAI 77, 84

Potekhin, A.Y., 1999, A&A 351, 787

Rogers, F. J., Iglesias, C. A., 1996, AAS 28, 915

Ritossa, C., Garcia–Berro, E., & Iben, I.Jr., (1999), Apj 515, 381

Siess, L., A &A 476, 893

Siess, L., A &A 497, 263

Tout, C.A., & Eldridge, J.J., 2004, MmSAI 75, 694